Analyst

PAPER

View Article Online
View Journal | View Issue

Cite this: *Analyst*, 2025, **150**, 4832

Additively manufactured microplate for the simultaneous colorimetric and electrochemical detection of atropine

Larissa M. A. Melo, [a,b] Elena Bernalte, [a] Robert D. Crapnell, [a] Matthew J. Whittingham, [a] Rodrigo A. A. Munoz, [c] Wallans T. P. dos Santos *[b,d] and Craig E. Banks *[a]

This work presents the development of a dual mode electrochemical and colorimetric sensing platform, produced in a single print through additive manufacturing. The cell design was based on the dimensions of a standard 96-well plate, with the base replaced by a disc electrode made from bespoke conductive polypropylene for the electrochemical testing, with the walls created from transparent non-conductive polypropylene to allow for the colorimetric tests. This new system was employed for the detection of atropine (ATP) in two distinct steps within the same electrochemical cell: (1) colour changes due to the reaction of ATP with bromocresol green, allowing for preliminary visual identification, and (2) the analysis of the electrochemical behaviour of the system before and after the colour change, providing quantitative confirmation. Both steps were performed in the same cell, highlighting the efficiency and practicality of the developed device. Wide linear ranges were obtained using square-wave voltammetry for ATP detection, spanning 0.65 to 20.83 mg mL^{-1} before the colorimetric reaction, and 5.21 to 20.83 mg mL^{-1} after the colorimetric reaction. Detection and quantification limits were calculated as 0.15 mg mL^{-1} and 0.50 mg mL^{-1}, respectively, demonstrating suitability for real application in forensic scenarios. Beverage samples (energy drink, tonic water, gin, gin with tonic water, and whisky) and synthetic biological samples (saliva, urine, and vitreous humour) were spiked with ATP and analysed using the proposed method, yielding recoveries close to 100%, indicating no matrix effect. This study demonstrates the synergy between additive manufacturing, and electrochemical and colorimetric sensing to create real, functional sensing platforms that are applicable to a wide range of fields.

Received 21st August 2025,
Accepted 24th September 2025

DOI: 10.1039/d5an00897b

rsc.li/analyst

1. Introduction

The development of dual-mode electrochemical and colorimetric sensors represents a significant advancement in analytical technology, offering both quantitative precision and visual simplicity in a single platform. These sensors enhance reliability by providing cross-validated results through two independent detection mechanisms, making them especially valuable in point-of-care diagnostics, environmental monitoring, forensic scenarios and resource-limited settings. Combined colorimetric–electrochemical methods have previously been reported for a range of analytes,[1–3] including demonstrating the feasibility of detecting atropine (ATP) using bromocresol green (BG) in conjunction with screen-printed electrodes.[4] ATP is a tropane alkaloid widely used in medicine; however, at elevated doses it can induce severe toxic effects, including cardiovascular and neurological disturbances, and in extreme cases, death.[5] Owing to its toxic potential, ATP has been reported in attempted homicides.[6] In forensic contexts, the detection of ATP at toxic levels (exceeding 10 mg) is crucial for establishing the cause of intoxication and guiding therapeutic interventions.[7] Electrochemiluminescence has also been reported as an efficient approach for the detection of ATP.[8,9] The reactions involving these compounds are illustrated in Scheme 1. Despite these advances, existing approaches still require separate platforms to perform the dual analysis. As such, there remains a clear need for the development of a portable, integrated system suitable for forensic applications.

Integrating both sensing modes into a single print, *via* additive manufacturing, further amplifies their impact –

[a]*Faculty of Science and Engineering, Manchester Metropolitan University, Dalton Building, Chester Street, M1 5GD, Great Britain. E-mail: c.banks@mmu.ac.uk; Tel: +44(0)1612471196*
[b]*Department of Chemistry, Federal University of Vales do Jequitinhonha and Mucuri, Campus JK, 39100000, Diamantina, Minas Gerais, Brazil. E-mail: wallanst@ufvjm.edu.br*
[c]*Institute of Chemistry, Federal University of Uberlândia, 38400-902, Uberlândia, Minas Gerais, Brazil*
[d]*Department of Pharmacy, Federal University of Vales do Jequitinhonha and Mucuri, Campus JK, 39100000, Diamantina, Minas Gerais, Brazil*

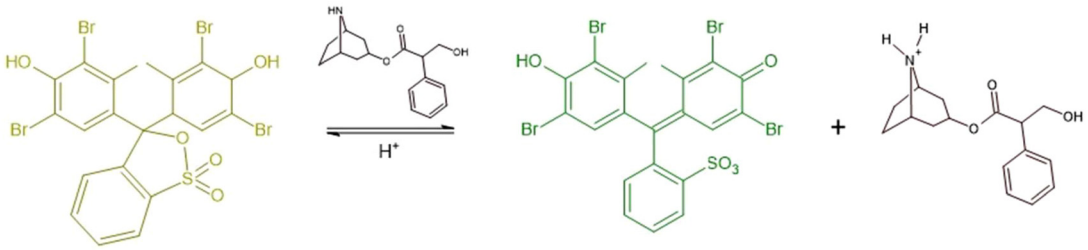

Scheme 1 Acid–base equilibrium of BG in the presence of ATP.[4]

enabling rapid, scalable, and cost-effective fabrication with minimal material waste. This approach not only streamlines production but also supports the creation of customizable, portable, and multifunctional devices *in situ*, aligning with the United Nations Sustainable Development Goal 9 of Industry, Innovation and Infrastructure.[10]

Additive manufacturing (also known as 3D-printing) is an exciting technology that has found popularity in many fields, both academic and industrial. One technique within additive manufacturing is Fused Filament Fabrication (FFF, also known as Fused Deposition Modelling or FDM), which has seen a rapid growth in popularity due to its low cost of entry and low cost of consumables. In general, additive manufacturing works through the sequential addition of layers of material in such a way to eventually create a 3-dimensional object, which was originally produced on a computer. For FFF, this involves the extrusion of millimetre lines of thermoplastic polymer, which are stacked in a layer-by-layer fashion. This form of manufacturing has garnered such attention due to some technological advantages and user flexibility it provides. These include the ability to produce complex part geometries with a high degree of customizability, short production times, low costs, and significantly lower waste production than the traditional formative and subtractive manufacturing counterparts.

One area where FFF has seen rapid growth is within electrochemistry, coined additive manufacturing electrochemistry. These techniques have a synergetic relationship whereby the cost of entry for both is low, and the possibility of adaptation/customization is high, leading to additive manufacturing being used to make equipment[11,12] and working electrodes.[13] Importantly, this synergy came about due to the commercial availability of electrically conductive filament, which embedded conductive carbon materials within poly(lactic) acid (PLA) filament. Through the use of these materials, a surge in the number of publications using additive manufacturing electrochemistry has been seen, including uses within sensing,[3,14–19] biosensing,[20–23] energy storage[24,25] and energy conversion.[26,27] This has allowed researchers to explore the novelty of both technologies. However, the electrochemical performance of such systems has remained poor, simply due to the limited conductivity of the available conductive filaments, which continues to hinder their viability for more practical or near to real applications. Recently, Gerroll *et al.*[28] demonstrated a high-throughput electrochemistry platform capable of automated analysis and synthesis, exemplifying the potential of integrated electrochemical systems.

Therefore, to elevate the implementation of additive manufacturing electrochemistry for real-world applications across different sectors, it is essential that several critical challenges are addressed. Firstly, the quality of conductive filament must be improved in two main ways: (i) the conductivity of the filament must be enhanced from the ~2–4 kΩ (across 10 cm of filament) seen for the most commonly utilized commercial conductive filament;[29] (ii) there needs to be a movement away from PLA due to limitations with chemical stability and processability of this polymer.[30] There have been numerous publications looking at improving the first of these issues, as researchers have taken to producing their own lab made filaments through either dissolving PLA within organic solvents and mixing in carbon allotropes,[31,32] or through thermally mixing PLA above its melting point to incorporate the conductive filler.[33,34] The second of these methodologies is seen to be most favourable due to the shorter production time (5 min rather than hours), the removal of hazardous solvents, and the possibility of powering machinery with green energy.[35,36] Secondly, due to the gap between academic research and commercial development, the design of real-life technologies for specific applications has been very limited. Instead the focus has remained on developing new materials, rather than translating these innovations into practical solutions.[37]

Regarding the electrochemical performance of additive manufactured sensors, researchers have focused on optimizing treatments to improve the performance of the electrodes produced using commercial conductive filament, including printing parameters,[38–42] design parameters[43,44] and surface modification of the post-printed parts.[45–49] While these have been important steps to advance in the field, attention has recently turned to the development of bespoke filaments to provide with improved and competitive alternatives. In this regard, there have been reports of bespoke filaments that improve the carbon loading, sustainability, and conductivity of the filaments.[50–52] In particular, within PLA, research have demonstrated that mixing conductive carbons of different morphologies can produce greatly enhanced conductivities[53] as well as filaments with similar electrochemical properties for a significantly lower material cost.[54] This goes a long way to solving the first problem with additive manufacturing electrochemistry; however, the backbone of the filament is still PLA.

Filaments produced from this polymeric material have been shown important limitations in their applicability due to solution ingress,[55] chemical stability,[30] and lack of consistent performance after sterilization,[56] which is vital within the healthcare industries.

To this end, researchers have recently moved toward other polymers capable of being used within additive manufacturing, such as thermoplastic polyurethane (TPU)[57] or poly(ethylene terephthalate glycol) (PETg).[56,58] The latter showed a significant reduction in solution ingress and an impressive stability in electrochemical signal after sterilization through ethanolic and UV radiation routes. Although both filaments reported using PETg are significant improvements on the current commercially available PLA, they do not reach the same conductivities of the bespoke PLA found within literature.[53] This is the case even though significantly more expensive conductive carbon allotropes are used. The use of three carbon allotropes (carbon black, graphene and multi-walled carbon nanotubes) within these filaments could be a step back in their commercialization due to both their material cost and difficulties their printability. More recently, conductive poly(propylene) (PP) filament has been first reported,[59,60] showing that up to 40 wt% of carbon black can be incorporated into PP polymer to create a conductive filament. Although 40 wt% is possible, this work shows how 30 wt% filament also exhibits an excellent electrochemical performance, and a 10 wt% reduction in conductive component is clearly advantageous to commercial uptake. Most importantly, such conductive PP filament offers excellent chemical resistance, no significant ingress and is a commonly used polymer within a multitude of industries.

Therefore, in this work we propose the use of bespoke 30 wt% conductive PP filament for the production of a dual mode analytical sensor based on a microplate design, where we combine non-conductive and conductive PP in a single print. In this design, the electrode will be placed at the base of the cell with clear PP creating the cell (or well) allowing for combined colorimetric and electrochemical detection on the same platform. We have applied the developed additive manufactured PP microplate for the specific dual colorimetric and electrochemical detection of ATP after its reaction with BG within samples of great forensic interest. The integrated platform enables cross-validation within a single assay using the same sample volume, thereby reducing the risks of contamination, sampling errors, and analysis time, while improving reliability in field applications with minimal sample requirements, which is a feature particularly critical in forensic matrices such as vitreous humour. It represents a rapid screening alternative for *in situ* quantitative confirmation, requiring fewer handling steps and providing faster responses, in addition to minimising false positives and negatives through the combined colorimetric–electrochemical output. Moreover, the integrated 3D-printed device not only ensures dual response and minimal sample consumption but also offers portability and scalability. The single-print design reduces production costs, facilitates technology transfer, and supports reproducibility in field applications.[61]

2. Experimental

2.1. Chemicals and samples

Deionized water with a resistivity of ≥18.2 MΩ cm, sourced from a Milli-Q Integral 3 system (Millipore UK, Watford, UK), was used to prepare the solutions. Atropine (ATP) (purity >99.0%) and bromocresol green (BG) analytical standards (powder), sourced from Tokyo Chemical Industry (Oxford, UK), were solubilized in methanol at a concentration of 250 mg mL^{-1} and 50 mg mL^{-1}, respectively. These solutions were diluted in adequate supporting electrolytes for electrochemical analysis. Britton–Robinson (BR) buffer solution (0.1 mol L^{-1}) was prepared with boric, phosphoric, and acetic acids (purities >99.9%), and sodium hydroxide (1.0 mol L^{-1}) was used to adjust the pH values between 2.0 and 12.0. Borate, phosphate and BR buffer solutions (0.1 mol L^{-1}) at pH 8.0, with 10% methanol (v/v) were also evaluated as a supporting electrolyte for ATP detection, as well as different concentrations of phosphate buffer solution (PBS) (0.05, 0.1 and 0.2 mol L^{-1}) was studied to verify the influence of ionic strength within electrochemical experiments. Sodium hydroxide (NaOH) (0.5 mol L^{-1}) was used for the electrochemical activation of the working electrode. Solvents such as tetrahydrofuran (THF), chloroform (>99.8%) and ethyl acetate (>99.5%) were used and purchased from (Merck, UK). Carbon black (CB) was purchased from PI-KEM (Tamworth, UK). Poly(propylene) (PP, Sabic® CX03-81 Natural 00900) was purchased from Hardie Polymers (Glasgow, UK).

Ascorbic acid, citric acid, fructose and glucose were evaluated as potential interferents for ATP detection by the proposed method. All reagents were of analytical grade and were purchased from Sigma-Aldrich (Lancashire, UK). Synthetic urine was prepared as described by Laube *et al.*,[62] artificial saliva as described by Chao Qian *et al.*,[63] and artificial vitreous humour as described by Sachin S. Thakur.[64] Synthetic/artificial biological samples, along with beverage samples (gin, whiskey, tonic water, energy drink, and gin with tonic water), were spiked with 10 mg mL^{-1} of ATP for subsequent analysis.

2.2. Filament production

The 30 wt% carbon black polypropylene (CB/PP) filament was produced by mixing 7.5 g of carbon black and 17.5 g of PP pellets using a Thermo Haake Polydrive dynameter fitted with a Thermo Haake Rheomix 600 (Thermo-Haake, Germany) using Banbury rotors at 70 rpm for 5 min with temperature set to 210 °C. The resulting polymer mixture was allowed to cool before granulated using a Rapid Granulator 1528 (Rapid, Sweden) to achieve a finer particle size. The granulated PP was then processed through a Filabot EX2 Filament Extruder (Filabot, VA, United States), set at 210 °C, to create a 1.75 mm filament, which was cooled over an air-cooling path and collected onto a spool.

2.3 Additive manufacturing of electrodes and microplates

All computer designs and 3MF files in this manuscript were produced using Fusion 360® (Autodesk®, CA, United States). These files were sliced and converted to GCODE files in

PrusaSlicer (Prusa Research, Prague, Czech Republic). The additive manufactured electrodes and microplate wells were produced using fused filament fabrication (FFF) technology on a Prusa XL (Prusa Research, Prague, Czech Republic). All additive manufactured electrodes and devices were printed using identical printing parameters, namely a 0.4 mm nozzle with a nozzle temperature of 215 °C, a bed temperature of 100 °C, 100% rectilinear infill, 0.15 mm layer height, and print speed of 35 mm s^{-1}. Wells that will be eventually used as sensing cells were printed using a 5T Prusa XL tool-changer, utilizing 2 of its 5 extruders. Extruder 1 was loaded with the custom 30 wt% CB/PP filament, while extruder 2 was loaded with BASF Ultrafuse PP. PrusaSlicer was used to prepare the file for printing, shown in Fig. S1, with settings adjusted to a 0.2 mm layer height, 2 perimeters per walls, 3 top/bottom layers, and 100% rectilinear infill. A 5 mm brim was added, along with a 0.3 mm first layer height, to enhance bed adhesion. The nozzle and bed temperatures were set to 240 °C and 70 °C, respectively. Magigoo PP was applied to the Prusa Smooth PEI build plate to improve the adhesion of the PP filaments.

2.4. Instrumental and apparatus

For the physicochemical characterization of the additive manufactured electrodes, X-ray Photoelectron Spectroscopy (XPS), Scanning Electron Microscopy (SEM) and Raman spectroscopy were applied.

XPS data were acquired using an AXIS Supra (Kratos, UK), equipped with a monochromatic Al X-ray source (1486.6 eV) operating at 225 W and a hemispherical sector analyser. It was operated in fixed transmission mode with a pass energy of 160 eV for survey scans and 20 eV for region scans with the collimator operating in slot mode for an analysis area of approximately 700 × 300 μm, the FWHM of the Ag 3d5/2 peak using a pass energy of 20 eV was 0.613 eV. The binding energy scale was calibrated by setting the graphitic sp^2 C 1s peak to 284.5 eV; this calibration is acknowledged to be flawed[65] but was nonetheless used in the absence of reasonable alternatives, and because only limited information was to be inferred from absolute peak positions.

SEM micrographs were obtained using a Crossbeam 350 Focussed Ion Beam – Scanning Electron Microscope (FIB-SEM) (Carl Zeiss Ltd, Cambridge, UK) fitted with a field emission electron gun. Secondary electron imaging was completed using a Secondary Electron Secondary Ion (SESI) detector. Energy Dispersive X-ray Spectroscopy (EDX) analysis was performed using an Ultim Max 170 detector (Oxford Instruments plc, Abingdon, UK) installed on the FIB-SEM. An acceleration voltage of 20 kV was used to image samples for EDX analysis experiments. Samples were mounted on the aluminium SEM pin stubs (12 mm diameter, Agar Scientific, Essex, UK) using adhesive carbon tabs (12 mm diameter, Agar Scientific, Essex, UK) and coated with a 5 nm layer of Au/Pd metal using a Leica EM ACE200 coating system before imaging. Quantification of EDX spectra was carried out using a standardless quantification procedure developed by Oxford Instruments and integrated into the AZtec 6.1 (Oxford Instruments, Abingdon, UK).

Raman spectroscopy was performed on a DXR Raman Microscope (Thermo Scientific Inc., Waltham, MA, USA) configured with a 532 nm laser and operates using OMNIC 9 software.

For the electrochemical experiments, a PGSTAT 204 potentiostat (Metrohm Autolab BV, Utrecht, Netherlands) controlled by NOVA 2.1. The electrochemical behaviour of ATP and BG was first characterized using standalone 30 wt% CB/PP additive manufactured electrodes with a lollipop-like shape to facilitate benchmarking (Fig. S2–S9) that were produced in-house, featuring a 0.55 cm^2 working electrode, a nichrome auxiliary electrode, and a refillable miniature Ag/AgCl reference electrode (ET073-1, EDAQ, Australia). The same system was employed in subsequent experiments in the microplate format, with the auxiliary and reference electrodes inserted through the top (open) of each well.

Before each measurement, the CB/PP was electrochemically activated using 0.5 mol L^{-1} NaOH and chronoamperometry: applying +1.6 V and −1.4 V for 150 s each, as widely described in the literature for the activation of additive manufactured electrodes.[66] The electrochemical studies were performed using cyclic voltammetry (CV) at CB/PP with different scan rates and pH values. ATP detection was optimized using the square-wave voltammetry (SWV) technique with 50 mV amplitude, 10 mV step potential and 10 Hz frequency parameters. Voltammograms obtained by SWV underwent background subtraction using polynomial fit in OriginPro 2016 software. Electrochemical measurements were conducted before and after the colorimetric reaction with BG.

For the electrochemical analyses, ATP standards/samples were consistently diluted in 0.1 mol L^{-1} PBS at pH 8.0. Colorimetric reaction (CR) was performed in the designed polypropylene additive manufactured microplates by mixing 50 μL of ATP stock solution or methanol (blank) with 10 μL of BG solution and then diluting (10 times) in PBS for further electrochemical analysis within the same platform. Note that, a yellow colour indicated the absence of ATP (negative reaction), while a colour change to green indicated the presence of ATP (positive reaction).

3. Results and discussion

3.1. Design and fabrication of the additive manufactured microplate

The microplate wells design was based on the dimensions of a standard laboratory 96-well plate, where the base of each well plate was replaced by an embedded lollipop electrode to allow dual colorimetric and electrochemical analysis. In this configuration, a single 6.5 mm diameter circular face of the electrode is exposed to solution. A previous layer of insulating PP was printed beneath the electrode connection points, to isolate the electrode within the cell and ensure the stability of the all-in-one print. Two different microplate designs were produced for testing, one containing one row of 10 individual wells and another one with 2 rows with 6 wells each, as illustrated in Fig. 1.

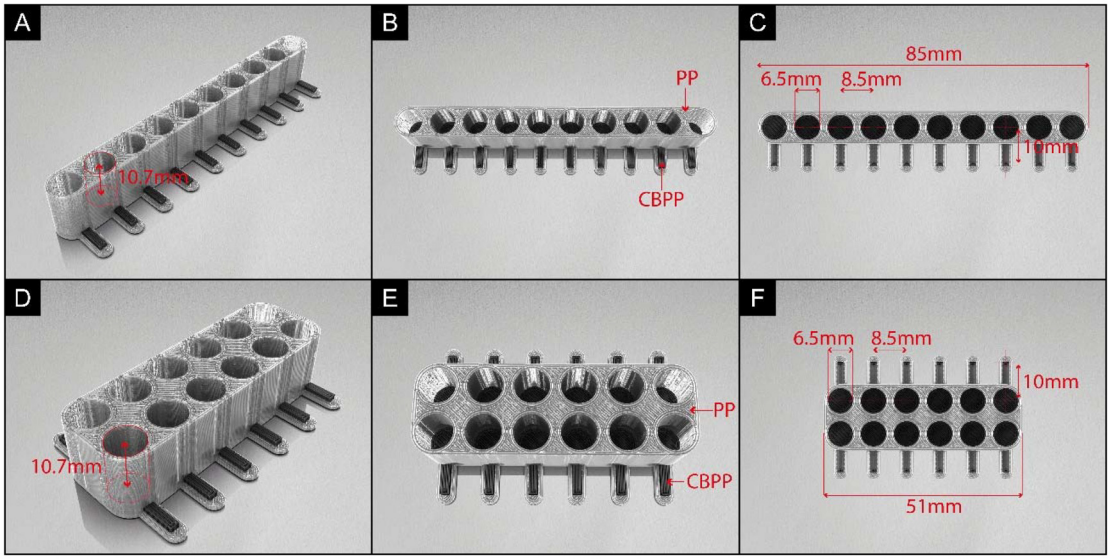

Fig. 1 (A–C) 1 × 10 and (D–F) 2 × 6 matrix cells with dimensions.

A standard polypropylene filament profile from BASF (Ultrafuse PP) was modified to limit the maximum volumetric flow rate of the extruders to 12 $mm^3\ s^{-1}$. This adjustment overrides the default print movement speeds to ensure consistent and accurate printing, as in-lab findings indicated inconsistencies in conductivity/resistivity between electrodes when using standard print profiles. Additionally, the reduced print speed improves layer-to-layer adhesion with PP, resulting in a watertight cell.

3.2. Electrochemical characterization

Firstly, surface activation methods for the CB/PP electrodes were investigated with the aim of exposing conductive carbon black particles embedded within or covered by the polymeric matrix, introducing oxygen-containing functional groups that facilitate electron transfer, and/or increasing the roughness/porosity of the electrode to improve the electrochemical response.[67] Mechanical (polishing), chemical (immersion), and electrochemical approaches, employing different solvents and reagents were evaluated and then tested the electrochemical performance of the additive manufactured electrode in an inner-sphere probe $[Fe(CN)_6]^{3-/4-}$ (1 mmol L^{-1} in 0.1 mol L^{-1} KCl), as shown in Fig. S2.

Mechanical polishing enables the removal of the superficial polymer layer and processing residues, thereby exposing conductive particles and increasing the electroactive surface area. Electrochemical activation in alkaline medium (NaOH) is a well-established procedure for carbon-based electrodes, as it promotes both structural reorganisation of the surface and the introduction of oxygenated groups, resulting in enhanced wettability and improved electron-transfer kinetics.[66] Treatments with strong acids, such as HNO_3 and H_2SO_4, are classically applied to functionalise carbon surfaces by generating carboxylic, carbonyl, and hydroxyl groups.[68,69] In contrast, the use of aqua regia, although an extremely strong oxidising agent, is limited by its aggressive nature and the potential degradation of the polymer matrix. Finally, organic solvents such as THF, chloroform, and ethyl acetate may induce swelling or promote the removal of surface additives from the polymer.[70] Each of these activation strategies therefore provides distinct contributions, whether by exposing conductive sites, introducing surface functionalities, or removing interfacial barriers, thus enabling comparison and identification of the most effective treatment for the intended analytical application.

The following methods were tested: electrode without treatment; after immersion in aqua regia (10 min and 24 h); polishing with sandpaper; chronoamperometry in NaOH solution; polishing + chronoamperometry in NaOH solution; 10 CV scans in sulfuric acid; 10 CV scans in nitric acid; after immersion in THF/chloroform (10 min) and in ethyl acetate (10 min). Note that the electrochemical characterization was performed using standalone lollipop electrodes in a standard electrochemical setup using nichrome wire and Ag/AgCl as counter and reference electrodes, respectively.

As depicted in Fig. S2, the best activation was achieved using NaOH, as determined by the $[Fe(CN)_6]^{3-/4-}$ electrochemical response, using ΔE_p (peak potential anodic–peak potential cathodic) and I_{pa}/I_{pc} ratios as evaluation, *i.e.*, greater reversibility of the redox processes. For further information regarding the filament and electrode resistances, and electrochemical characterisation of conductive PP electrodes with this filament composition, such as outer-sphere probes, we refer readers to previously published work.[59,60] To assess the activation for ATP detection, the chronoamperometry parameters were evaluated and optimised, seeking the best analytical response in terms of the highest peak current and the smallest peak width at half height. The parameters tested included anodic potential +1.0, +1.2, +1.4 and +1.6 V, cathodic

potential −1.2, −1.0, −0.8 and −0.6 V and application time 50, 100, 150, 200 and 250 s. The results of the cyclic voltammograms (CV) recorded in 20 mg mL^{-1} ATP at CB/PP in 0.1 mol L^{-1} PBS (pH 8.0) after applying different activation conditions resulted in the optimal parameters achieved at +1.6 V and −1.4 V for 150 s each, as shown in Fig. S3.

To evaluate the effect of the optimised activation method on the electron transfer kinetics and electrochemical surface area of the additive manufactured electrode, scan rate study was next performed against the commonly used inner-sphere probe $[Fe(CN)_6]^{3-/4-}$ (1 mmol L^{-1} in 0.1 mol L^{-1} KCl), enabling the determination of the heterogeneous electron transfer rate constant (k^0) at 6.6. × 10^{-5} cm s^{-1} and the real electrochemical surface area (A_e) at 0.17 (±0.04) cm^2. These results demonstrate that the material is electroactive and suitable for use as a working electrode in analytical applications, showing agreement with previous work.[59]

3.3. Physicochemical characterization

Then, a physicochemical characterization of the laboratory-produced electrodes before and after activation was performed using X-ray photoelectron spectroscopy (XPS), Raman spectroscopy and scanning electron microscopy (SEM), Fig. 2.

The laboratory-produced CB/PP filament utilized for fabricating the new dual colorimetric/electrochemical microplate demonstrated high low temperature flexibility (Fig. 2A) showing its suitability for 3D-printing. Raman characterization of CB/PP before and after activation was performed, and the spectra are presented in Fig. 2D. The electrodes, both before and after NaOH activation, exhibited characteristic Raman bands: D (~1352 cm^{-1}), G (~1599 cm^{-1}), and 2D (~2889 cm^{-1}), typical of graphitic-like structures. Hydrocarbon polymers such as PP exhibit intense C–H stretching bands in the region of approximately 2800–3000 cm^{-1} (symmetric and asymmetric CH_2/CH_3 stretches).[71] In Raman spectra of PP and other polyolefins, these modes typically appear at ≈2850 cm^{-1} (symmetric CH_2), ≈2875–2885 cm^{-1} (symmetric CH_3), and ≈2920–2950 cm^{-1} (asymmetric CH_3 stretches).[72] Given that our electrodes are composed of CB dispersed in a PP matrix, a band near 2800 cm^{-1} is consistent with a contribution from the polymer or from adsorbed organic species/solvent residues. It is also important to note that carbonaceous materials (graphite, graphene, carbon black) display harmonic and second-order combination bands in the high-frequency region. The well-known 2D (G′) band appears near 2700 cm^{-1}, with its position dependent on excitation wavelength. In addition, combination bands such as D + G (commonly reported at ≈2940–2950 cm^{-1}) and other second-order features have been observed in disordered graphitic carbons.[73] Thus, a genuine carbon-derived overtone or combination could also give rise to features in the 2800–3000 cm^{-1} range, particularly in disordered materials or under excitation conditions that favour double-resonance processes. The calculated I_D/I_G ratios were 1.07 for CB/PP as printed and 1.09 for CB/PP activated, indicating a degree of structural disorder in the graphitic materials due to the pronounced intensity of the D band, and confirm the CB presence.

These findings are consistent with SEM images of the CB/PP electrodes before (Fig. 2B) and after activation (Fig. 2C). The untreated electrode exhibited a typical carbonaceous morphology, in contrast, the activated electrode displayed partial layer removal with several perforations (Fig. S4), exposing more

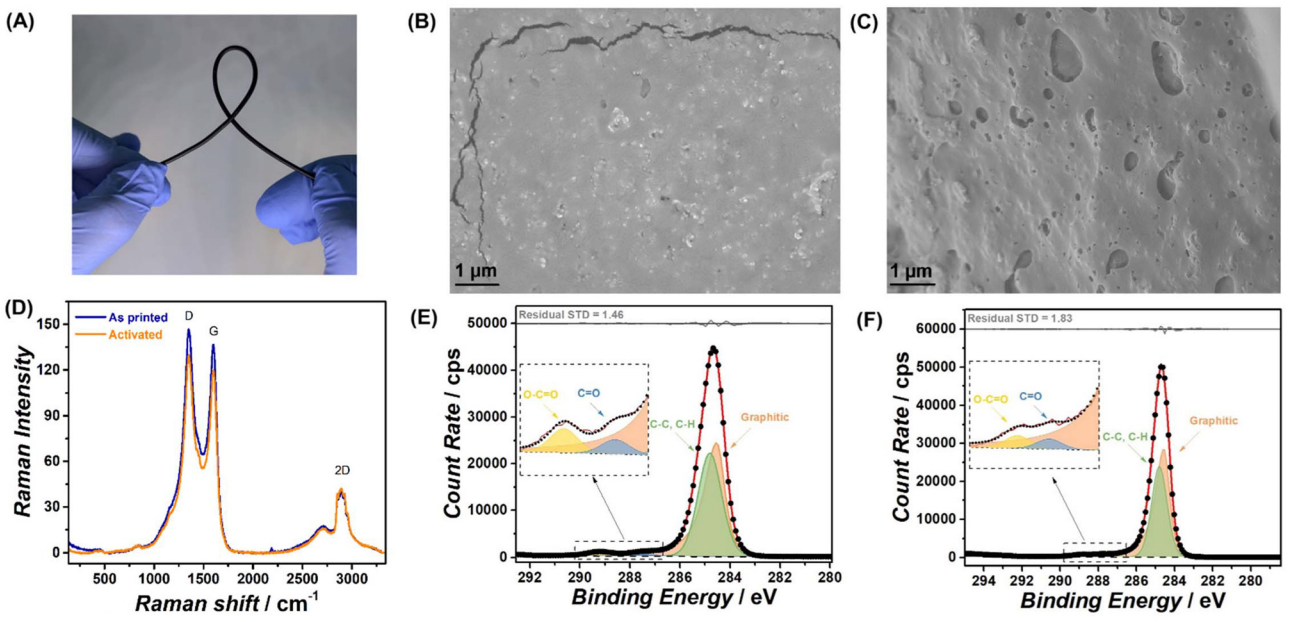

Fig. 2 (A) Photograph highlighting the flexibility of the 30 wt% CB/PP. SEM micrographs for the surface of the CB/PP (B) before and (C) after activation at 15k magnification. (D) Raman spectra for CB/PP as printed in blue and activated in orange. XPS C 1s spectra for the (E) 30 wt% CB/PP as printed and (F) 30 wt% CB/PP activated.

conductive material. The combination of NaOH treatment and chronoamperometry notably expands potential weak spots on the electrode surface. This observation aligns with the XPS findings (Fig. 2E, F, and Table S1 – SI), which indicate an increase in surface graphitic carbon after activation (+4%). This structural change suggests enhanced electrochemical performance for the working electrode (WE) for detecting substances whose electrochemical behaviour depends on the electrode surface, such as inner-sphere probes.

3.4. Electroanalytical performance of ATP

Given that many psychotropic molecules, including ATP, are amine-based compounds, their detection in aqueous unbuffered solutions can significantly influence the local pH. This pH shift may interfere with colorimetric responses, particularly when using reagents such as bromocresol green (BG), potentially compromising signal intensity and colour definition. Therefore, investigating additionally the electrochemical behaviour of these colorimetric reactions, which will provide with another analytical validation of the reaction, becomes essential to ensure the robustness and accuracy of dual-mode sensing platforms in these scenarios.

Then, the electrochemical behaviour of ATP was evaluated in 0.1 mol L^{-1} BR buffer solution across a pH range from 2.0 to 12.0, both in the absence (A) and presence (B) of BG, after electrode activation with NaOH by chronoamperometry. Using CV at CB/PP in manufactured microplate, as shown in Fig. S5. ATP exhibits an irreversible oxidation process (O_1) at CB/PP, as depicted in Fig. S5A. In the presence of BG, the same O_1 is observed superimposed on the oxidation of BG itself (Fig. S5B).

The ATP redox process in CB/PP demonstrated a pH-dependent behaviour, with peak potential (E_p) shifting to more negative values as the pH increased. Fig. S6A and B show the plots of E_p and I_p (peak current) for the redox processes as a function of pH at CB/PP. Indicating that the redox processes of ATP involve protons, the lack of linearity observed with distinct behaviour at pH values above 9 is likely related to the pK_a values of this molecule (9.19 and 15.15). At pH levels above 9, ATP exists predominantly in its fully deprotonated amine form, which may account for the different behaviour observed under these conditions. For ATP detection, pH 8.0 was selected due to this pH, the oxidation processes of ATP and BG are very well differentiated (Fig. S7). Then, different supporting electrolytes, namely BR, borate, and PBS buffer solutions, were evaluated, and results are shown in Fig. S8. All three buffers tested produced the same oxidation peak for ATP at a similar potential, however, a clear difference in peak current was observed, with PBS buffer yielding the highest response – this behaviour can be attributed to specific interactions of phosphate at the electrode/electrolyte interface – and was therefore chosen as the supporting electrolyte for ATP detection. Under these conditions, various concentrations of PBS were subsequently tested to assess the influence of ionic strength, with 0.1 mol L^{-1} PBS being selected for its superior resolution of the observed redox processes (Fig. S9).

Attention was next turned to the assessment of the mass transport control of the redox process on the CB/PP surface, for what CV experiments were conducted at varying scan rates (v) in 20 mg mL^{-1} ATP in 0.1 mol L^{-1} PBS at pH 8.0 before and after colorimetric reaction (CR) (Fig. S10 and S11). The I_p for ATP before and after CR at CB/PP exhibited a stronger correlation with the square root of the scan rate (Fig. S10C and S11C) rather than with the scan rate itself (Fig. S10B and S11B), suggesting that the electrochemical processes are predominantly governed by diffusion on the CB/PP surface. The logarithmic plots of I_p *vs.* v display linear relationships (Fig. S10D and S11D), with the equations detailed in Table S2. The obtained slopes ($\leq$0.5) from these equations confirm diffusion-controlled processes. The observation of slopes lower than 0.5 in the log I_p *vs.* log v plots indicates that ATP oxidation is not governed solely by semi-infinite diffusion and instead reflects additional kinetic or chemical constraints. In this case, the irreversible nature of ATP oxidation implies slow heterogeneous electron transfer, while the subsequent reaction with BG may further reduce mobility. Such effects are consistent with quasi-reversible or electrochemical–chemical (EC-type) mechanisms, in which coupled chemical steps or surface fouling diminish the effective electroactive concentration, thereby limiting the current growth with scan rate.[74]

Fig. 3 illustrates the detection of ATP before and after the CR with BG using SWV, under optimal conditions (50 mV amplitude, 10 mV step potential, and 10 Hz frequency).[4] The identification of ATP by SWV detection can be performed through two analytical responses, since ATP presents a characteristic electrochemical behaviour on CB/PP electrode, with peak potentials at +0.60 and +0.78 V (*vs.* Ag/AgCl) before and

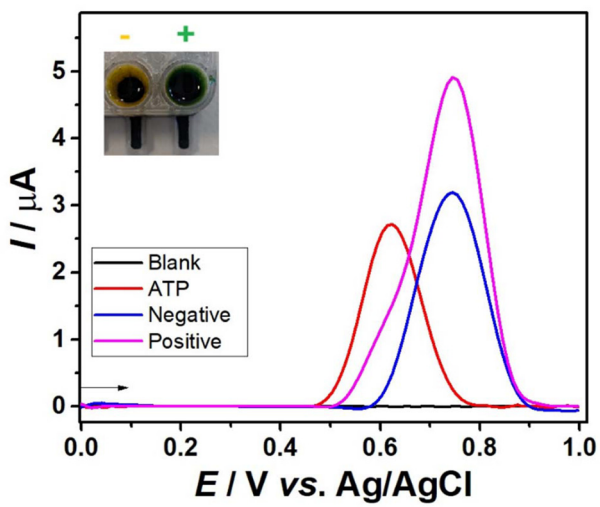

Fig. 3 SWV voltammograms of 0.1 mol L^{-1} PBS at pH 8.0 before (black line) and after addition of 20 mg mL^{-1} ATP (red line); and BG in absence (blue line) and in presence (magenta line) of ATP after CR (dilution 10×), at CB/PP. All potential scans started at 0.0 V. Experimental conditions: amplitude of 50 mV, step potential of 10 mV, and frequency 10 Hz. Inserted negative (yellow) and positive (green) results of the colorimetric test for ATP using BG.

after the CR, respectively. In the presence of BG, the ATP oxidation peak (O_1) decreased in current (magenta line) compared with ATP alone (red line), whereas the process involving BG showed increased peak currents in the presence of ATP compared with BG alone (blue line – negative control). This indicates a chemical interaction between ATP and BG, likely consuming ATP and altering the electrochemical behaviour of both species.[4] In addition, as shown in the inset of Fig. 3, the colour change resulting from the CR in the presence of BG is easily observed in the proposed additive manufactured microplate, which is also demonstrated from various perspectives in Fig. S12.

Note that to perform the dual colorimetric and electrochemical detection within the additive manufactured microplate, the colorimetric solution is added directly in the well and, after color changes, a dilution (10×) is made for the electrochemical analysis after CR. Following the optimization of conditions,[4] tests for repeatability and reproducibility were carried out using the same (N = 3) and different (N = 3) CB/PP electrodes, both prior to and after the CR by SWV, as detailed in Table S3.

Good stability was observed for the electrochemical responses of ATP and BG using the proposed method, both before and after the CR. The measurements of E_p and I_p exhibited low relative standard deviations (RSDs), with E_p showing RSDs under 0.5% and I_p under 10%. As detailed in Table S3, the consistency of ATP's E_p at CB/PP across all measurements, with RSDs below 0.5%, underscores the effectiveness of CB/PP with SWV as a reliable screening method for ATP detection. The linear range for ATP determination was assessed using standard solutions (0.65–20.83 mg mL^{-1}), shown in Fig. 4.

As shown in Fig. 4A, two linear ranges between 0.65–5.21 mg mL^{-1} (R^2 = 0.99) and 5.21–20.83 mg mL^{-1} (R^2 = 0.98) were obtained for ATP quantification using the proposed method before CR. While after CR a linear range between 5.21–20.83 mg mL^{-1} (R^2 = 0.99) was obtained, as demonstrated in Fig. 4B. The difference in the number of calibration points between Fig. 4A and B arises from the linear dynamic range obtained in each case. The presence of two linear regions for ATP before the CR (Fig. 4A) can be attributed to phenomena commonly observed in electrochemical measurements with additively manufactured electrodes. At low concentrations, the current is proportional to the concentration under diffusion-controlled conditions, whereas at higher concentrations, partial surface saturation or adsorption effects may reduce the effective electron-transfer rate, resulting in a second linear region with a different slope. Furthermore, the heterogeneity of CB/PP electrodes, including variations in surface roughness, incipient porosity, and conductive carbon distribution, can create areas with differing electrochemical activity, further contributing to the observation of two linear regions.[74] The linear regression equations for these processes are also summarized in Table S4.

It is worth mentioning that all the analysed concentrations were detectable by the colorimetric technique. A limit of detection (LOD) and a limit of quantification (LOQ) were calculated as 0.15 mg mL^{-1} and 0.50 mg mL^{-1}, respectively, using IUPAC definitions of $3 \times S_B/m$ and $10 \times S_B/m$, where S_B represents the standard deviation of the background response, and m is the slope of the linear regression. Atropine concentrations in forensic samples vary considerably depending on the clinical or post-mortem context. In human plasma, therapeutic levels are typically in the range of 1–8 ng mL^{-1} following controlled administration, whereas cases of acute intoxication have reported concentrations as high as 0.3 mg mL^{-1}. In fatal cases, blood concentrations between 0.5 and 0.9 mg mL^{-1}, and urinary concentrations of approximately 0.7 mg mL^{-1}, have been described.[75–77] It is noteworthy that the LOD, LOQ, and linear ranges determined by the proposed method are sufficiently low for application to forensic samples suspected of containing lethal doses of ATP (≥10 mg mL^{-1}).[78]

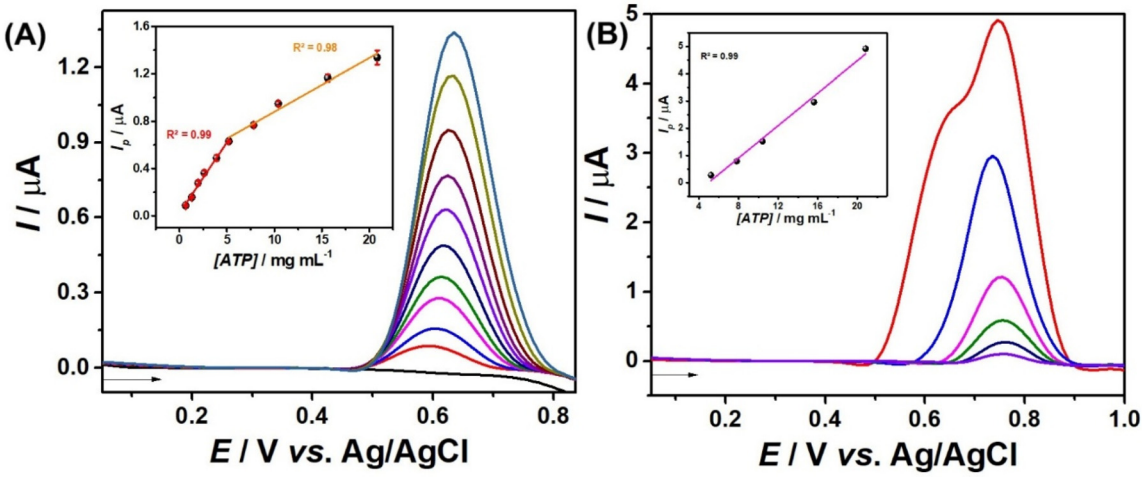

Fig. 4 SWV voltammograms in 0.1 mol L^{-1} PBS at pH 8.0 at CB/PP (A) before and (B) after CR with 0.65–20.83 mg mL^{-1} ATP. Experimental conditions: amplitude of 50 mV, step potential of 10 mV, and frequency 10 Hz. Inset show linear regression. All measurements were performed in triplicate, and the error bars were smaller than the symbol presented in the inset.

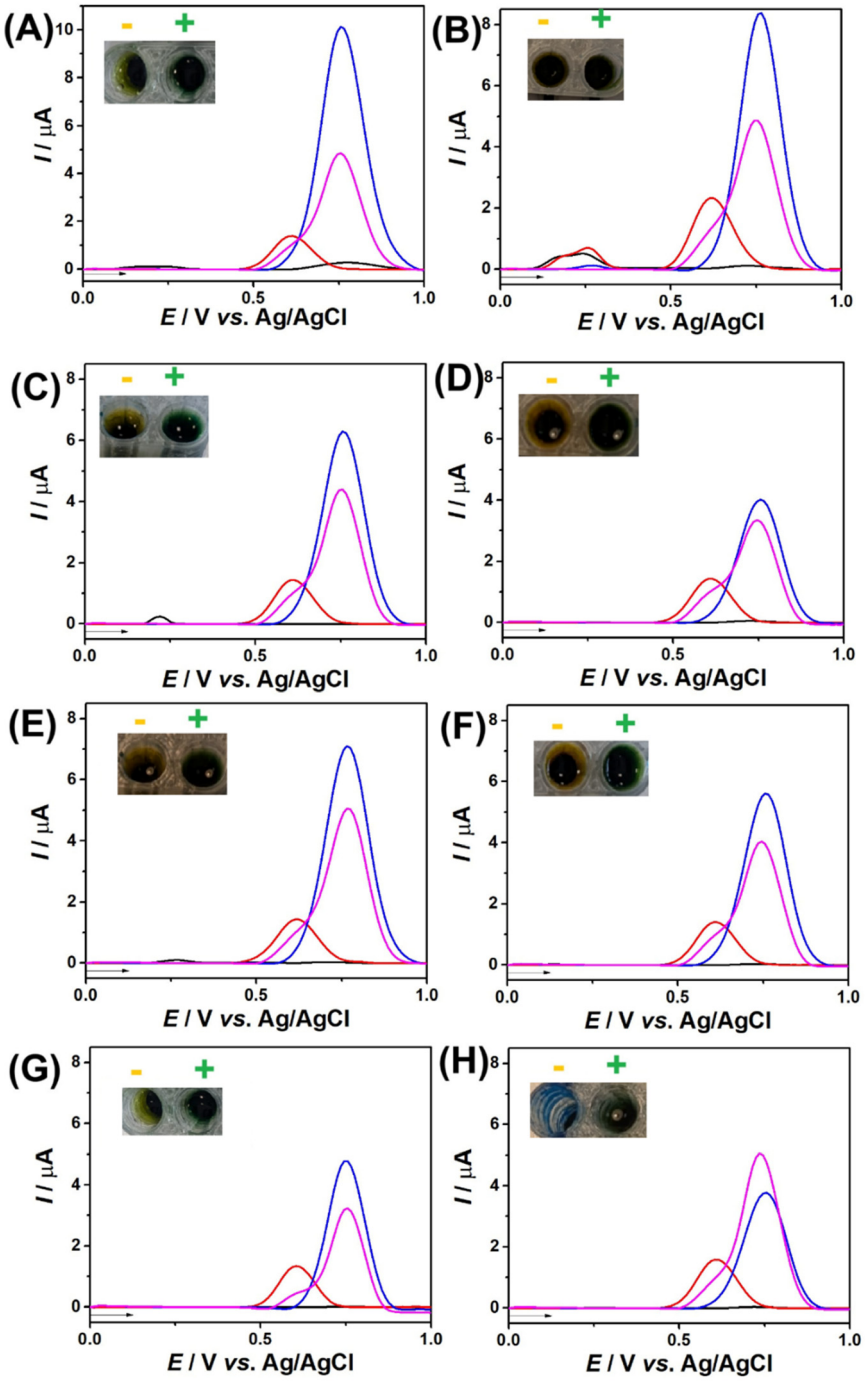

Fig. 5 SWV voltammograms of 0.1 mol L^{-1} PBS at pH 8.0 before (black line) and after addition of 20 mg mL^{-1} ATP (red line); and BG in absence (blue line) and in presence (magenta line) of ATP after CR (dilution 10×), at CB/PP. In (A) energy drink, (B) tonic water, (C) gin, (D) gin with tonic water, (E) whisky, (F) saliva, (G) urine and (H) vitreous humour. All potential scans started at 0.0 V. Experimental conditions: amplitude of 50 mV, step potential of 10 mV, and frequency 10 Hz. Inserted negative (yellow) and positive (green) results of the colorimetric test for ATP using BG.

3.5. Electroanalytical application

The proposed method was applied to metabolites typically found in biological samples and to potential interferents in beverage samples, including ascorbic acid (AA), citric acid (CA), glucose (GLU), and fructose (FRU). These results are presented in Fig. S13, both before and after CR, with the colorimetric test results for these compounds shown at the inset of the figures – to enhance photographic clarity of the colour (yellow), the solutions were placed in a transparent microplate. A comparison of the electrochemical signal of ATP before and after CR is also provided in all graphs (red line). Fig. S13 illustrates that under

the conditions of the proposed method, oxidation was observed solely for AA, both prior to and following CR. However, the E_p identified for AA at +0.35 V (*vs.* Ag/AgCl) is distinct enough to ensure precise ATP detection without peak overlap. This demonstrates that the electrochemical process, both before and after CR, supports selective ATP analysis. Moreover, the colorimetric step clearly exhibits high selectivity for ATP when compared to the other compounds analysed. Some samples that may be of interest for ATP detection in forensic analysis were doped with 20 mg mL^{-1} ATP, analysed by the proposed method and are shown in Fig. 5, the recoveries are shown in Table S5 for before and after the CR. To better visualize the colour change in photographs, the solutions were also transferred to a transparent microwell plate, as shown in Fig. S14.

As shown in Fig. 5, ATP behaviour in all samples studied was consistent with that of the standard, indicating no significant matrix effect. The colorimetric step was also highly selective, with a clear colour change observed. It is worth noting that in vitreous humour samples, the negative control in the colorimetric test displayed a blue coloration, likely due to the pH of the sample. However, the colour change to green in the presence of ATP was clearly evident. The additional peaks observed in Fig. 4A–C and E, between 0.1 and 0.3 V (*vs.* Ag/AgCl), are likely due to redox-active components present in the different matrices. In energy drinks, such peaks may originate from caffeine, taurine, ascorbic acid, or other antioxidants. In tonic water, quinine is a known electroactive species within this potential range.[79,80] In gin and whisky, phenolic compounds, aldehydes, and other minor constituents from botanical additives or barrel ageing (*e.g.*, tannins[81] and vanillin[82]) may contribute to additional oxidation processes. Variations in signal intensity between matrices are consistent with differences in the composition of these electroactive interferents, such as quinine in tonic water, as well as their interactions with the CB/PP electrode surface, contributing to recoveries below 90% (like gin and gin with tonic water) or above 110% (tonic water) (Table S5). Despite these, the combined method can be efficiently applied for the detection and quantification of ATP using the colorimetric response and the electrochemical signals measured both before and after the CR, thus providing three independent analytical responses.

A comparison of the principal analytical parameters for ATP detection by voltammetry is presented in Table S6. Compared with existing methods, the proposed method exhibits a favourable linear range and a low LOD. Although it does not achieve the highest values, these parameters are still adequate for applications in real samples. Furthermore, it constitutes a unique dual-response platform, combining colorimetric and electrochemical detection, providing three independent analytical responses.

4. Conclusions

This work reports the production of a dual mode, portable, electrochemical and colorimetric sensing platform in a microplate design that can be produced in a single print using transparent non-conductive polypropylene filament and a bespoke conductive filament containing 30 wt% carbon black. This configuration not only increases the sensitivity and reproducibility of the detection process but also facilitates simultaneous colorimetric and electrochemical analysis within the same cell. The method employs the CB/PP electrode for the rapid and sensitive detection of ATP in biological and beverage samples, achieving an LOD of 0.151 mg mL^{-1}. The process begins with the electrochemical response of ATP prior to the CR, followed by an analysis of the ATP-induced color change using BG and subsequent electrochemical evaluation of the same solution. The use of the innovative CB/PP electrode and 3D-printed cell enhances the portability and miniaturization of the method, making it ideal for on-site forensic analysis. This method has proven reliable for forensic samples, demonstrating good stability (RSD <0.5% for E_p and <10% for I_p) with consistent results across different electrodes. The introduction of this 3D-printed material and cell configuration marks a significant advancement, providing a fast, reliable, and practical tool for real-world applications whilst being clearly applicable to many forms of sensing applications including forensics, environmental analysis and point-of-care diagnostics.

Conflicts of interest

There are no conflicts of interest to declare.

Data availability

All data is shown in the paper. Authors are required to contact the corresponding author for raw files/imagines.

Supplementary information (SI) is available. See DOI: https://doi.org/10.1039/d5an00897b.

Acknowledgements

The authors would like to acknowledge the help of Dr Hayley Andrews and Dr Yibing Zhu for the acquisition of Raman and SEM data, respectively. The authors would like to acknowledge INCT-SP (CNPq/406958/2022-0, FAPEMIG/APQ-03984-24, and CAPES/88887.954256/2024-00, 88887.836030/2023-00 and financial code 001), CNPq (313367/2021-3), FAPEMIG [APQ-01996-23 and RED-00120-23]. CAPES (88887.639849/2021-00, 88887.014930/2024-00 and 88881.934755/2024-01) and Horizon Europe (grant 101137990) for their funding.

References

1 S. Dortez, M. Pacheco, T. Gasull, A. G. Crevillen and A. Escarpa, *Lab Chip*, 2024, **24**, 4253–4263.
2 M. O. Arrieiro, L. C. Arantes, E. M. Richter, R. A. Muñoz and W. T. dos Santos, *Microchem. J.*, 2024, **201**, 110717.

3 L. M. Melo, L. V. de Faria, L. C. Arantes, E. M. Richter, R. A. Munoz and W. T. dos Santos, *Electrochim. Acta*, 2024, **483**, 144041.
4 L. M. Melo, E. Bernalte, R. D. Crapnell, R. M. Verly, R. A. Muñoz, W. T. dos Santos and C. E. Banks, *Sens. Actuators, B*, 2025, 137962.
5 G. Koželj, L. Perharič, L. Stanovnik and H. Prosen, *J. Pharm. Biomed. Anal.*, 2014, **96**, 197–206.
6 A. C. Gören, G. Bilsel, M. Bilsel, S. Yenisoy-Karakaş and D. Karakaş, *J. Chromatogr., A*, 2004, **1057**, 237–239.
7 P. Boermans, H. Go, A. Wessels and D. Uges, *Ther. Drug Monit.*, 2006, **28**, 295–298.
8 Y. Xiu-Yun, X. Chun-Ying, Y. Bai-Qing and Y. Tian-Yan, *Chin. J. Anal. Chem.*, 2011, **39**, 1233–1237.
9 K. Brown, M. McMenemy, M. Palmer, M. J. Baker, D. W. Robinson, P. Allan and L. Dennany, *Anal. Chem.*, 2019, **91**, 12369–12376.
10 U. Nations, The 17 Goals, **https://sdgs.un.org/goals**, (accessed 06/04/2023).
11 C. Scheid, S. A. Monteiro, W. Mello, M. C. Velho, J. Dos Santos, R. C. R. Beck, M. Deon and J. Merib, *J. Chromatogr., A*, 2024, **1722**, 464892.
12 M. J. Whittingham, R. D. Crapnell and C. E. Banks, *Anal. Chem.*, 2022, **94**, 13540–13548.
13 A. G.-M. Ferrari, N. J. Hurst, E. Bernalte, R. D. Crapnell, M. J. Whittingham, D. A. Brownson and C. E. Banks, *Analyst*, 2022, **147**, 5121–5129.
14 M. Di-Oliveira, D. A. Araújo, D. L. Ramos, L. V. de Faria, R. G. Rocha, R. M. Sousa, E. M. Richter, T. R. Paixão and R. A. Munoz, *Electrochim. Acta*, 2024, **481**, 143945.
15 A. dos Santos Novais, D. G. Ribeiro, L. M. de Almeida Melo, E. F. Júnior, L. C. Arantes, B. G. Lucca, E. I. de Melo, R. F. Brocenschi, W. T. P. dos Santos and R. A. B. da Silva, *Sens. Actuators, B*, 2024, **398**, 134667.
16 T. P. Lisboa, G. F. Alves, L. V. de Faria, C. C. de Souza, M. A. C. Matos and R. C. Matos, *Talanta*, 2022, **247**, 123610.
17 L. M. Melo, L. V. de Faria, L. C. Arantes, D. A. Alves, C. M. Rocha, Â. de Fátima, R. A. Munoz, E. M. Richter and W. T. Dos Santos, *Talanta*, 2024, **276**, 126237.
18 D. P. Rocha, A. L. Squissato, S. M. da Silva, E. M. Richter and R. A. Munoz, *Electrochim. Acta*, 2020, **335**, 135688.
19 J. G. Walters, S. Ahmed, I. M. Terrero Rodríguez and G. D. O'Neil, *Electroanalysis*, 2020, **32**, 859–866.
20 R. D. Crapnell and C. E. Banks, *Anal. Methods*, 2024, **16**, 2625–2634.
21 C. Kalinke, P. R. de Oliveira, B. C. Janegitz and J. A. Bonacin, *Sens. Actuators, B*, 2022, **362**, 131797.
22 C. Kalinke, N. V. Neumsteir, P. R. de Oliveira, B. C. Janegitz and J. A. Bonacin, *Anal. Chim. Acta*, 2021, **1142**, 135–142.
23 J. Muñoz and M. Pumera, *TrAC, Trends Anal. Chem.*, 2020, **128**, 115933.
24 K. Ghosh and M. Pumera, *Small Methods*, 2021, **5**, 2100451.
25 K. Ghosh and M. Pumera, *Nanoscale*, 2021, **13**, 5744–5756.
26 M. P. Browne, V. Urbanova, J. Plutnar, F. Novotný and M. Pumera, *J. Mater. Chem. A*, 2020, **8**, 1120–1126.
27 B. Hüner, N. Demir and M. F. Kaya, *Fuel*, 2023, **331**, 125971.
28 B. H. Gerroll, K. M. Kulesa, C. A. Ault and L. A. Baker, *ACS Meas. Sci. Au*, 2023, **3**, 371–379.
29 M. Goutier, K. Hilbig, T. Vietor and M. Böl, *Polymers*, 2023, **15**, 2159.
30 K. S. Erokhin, E. G. Gordeev and V. P. Ananikov, *Sci. Rep.*, 2019, **9**, 20177.
31 J. S. Stefano, L. R. G. e. Silva, R. G. Rocha, L. C. Brazaca, E. M. Richter, R. A. A. Muñoz and B. C. Janegitz, *Anal. Chim. Acta*, 2022, **1191**, 339372.
32 J. S. Stefano, L. R. G. e. Silva and B. C. Janegitz, *Microchim. Acta*, 2022, **189**, 414.
33 I. V. Arantes, R. D. Crapnell, M. J. Whittingham, E. Sigley, T. R. Paixão and C. E. Banks, *ACS Appl. Eng. Mater.*, 2023, **1**, 2397–2406.
34 P. Wuamprakhon, R. D. Crapnell, E. Sigley, N. J. Hurst, R. J. Williams, M. Sawangphruk, E. M. Keefe and C. E. Banks, *Adv. Sustainable Syst.*, 2023, **7**, 2200407.
35 R. D. Crapnell and C. E. Banks, *Green Carbon*, 2023, **1**, 85–93.
36 R. D. Crapnell, C. Kalinke, L. R. G. Silva, J. S. Stefano, R. J. Williams, R. A. A. Munoz, J. A. Bonacin, B. C. Janegitz and C. E. Banks, *Mater. Today*, 2023, **71**, 73–90.
37 W. B. Veloso, T. R. Paixão and G. N. Meloni, *Anal. Chem.*, 2024, **96**, 14315–14319.
38 E. Bernalte, R. D. Crapnell, O. M. Messai and C. E. Banks, *ChemElectroChem*, 2024, **11**, e202300576.
39 H. H. Bin Hamzah, O. Keattch, D. Covill and B. A. Patel, *Sci. Rep.*, 2018, **8**, 9135.
40 C. Iffelsberger, C. W. Jellett and M. Pumera, *Small*, 2021, **17**, 2101233.
41 R. S. Shergill, C. L. Miller and B. A. Patel, *Sci. Rep.*, 2023, **13**, 339.
42 R. S. Shergill and B. A. Patel, *ChemElectroChem*, 2022, **9**, e202200831.
43 R. D. Crapnell, A. Garcia-Miranda Ferrari, M. J. Whittingham, E. Sigley, N. J. Hurst, E. M. Keefe and C. E. Banks, *Sensors*, 2022, **22**, 9521.
44 C. Miller, O. Keattch, R. S. Shergill and B. A. Patel, *Analyst*, 2024, **149**, 1502–1508.
45 M. P. Browne, F. Novotny, Z. k. Sofer and M. Pumera, *ACS Appl. Mater. Interfaces*, 2018, **10**, 40294–40301.
46 C. Kalinke, N. V. Neumsteir, G. de Oliveira Aparecido, T. V. de Barros Ferraz, P. L. Dos Santos, B. C. Janegitz and J. A. Bonacin, *Analyst*, 2020, **145**, 1207–1218.
47 E. Redondo, J. Muñoz and M. Pumera, *Carbon*, 2021, **175**, 413–419.
48 D. P. Rocha, R. G. Rocha, S. V. Castro, M. A. Trindade, R. A. Munoz, E. M. Richter and L. Angnes, *Electrochem. Sci. Adv.*, 2022, **2**, e2100136.
49 R. S. Shergill, F. Perez, A. Abdalla and B. A. Patel, *J. Electroanal. Chem.*, 2022, **905**, 115994.
50 R. D. Crapnell, E. Sigley, R. J. Williams, T. Brine, A. Garcia-Miranda Ferrari, C. Kalinke, B. C. Janegitz, J. A. Bonacin and C. E. Banks, *ACS Sustainable Chem. Eng.*, 2023, **11**, 9183–9193.

51 E. Sigley, C. Kalinke, R. D. Crapnell, M. J. Whittingham, R. J. Williams, E. M. Keefe, B. C. Janegitz, J. A. Bonacin and C. E. Banks, *ACS Sustainable Chem. Eng.*, 2023, **11**, 2978–2988.
52 B. Ferreira, E. Bernalte, R. D. Crapnell, K. K. Augusto, U. Lomesh, M. A. Khan, O. Fatibello-Filho, T. R. Paixão and C. E. Banks, *ACS Appl. Eng. Mater.*, 2025, **3**, 1759–1769.
53 R. D. Crapnell, I. V. Arantes, J. R. Camargo, E. Bernalte, M. J. Whittingham, B. C. Janegitz, T. R. Paixão and C. E. Banks, *Microchim. Acta*, 2024, **191**, 96.
54 K. K. Augusto, R. D. Crapnell, E. Bernalte, S. Zighed, A. Ehamparanathan, J. L. Pimlott, H. G. Andrews, M. J. Whittingham, S. J. Rowley-Neale and O. Fatibello-Filho, *Microchim. Acta*, 2024, **191**, 375.
55 R. J. Williams, T. Brine, R. D. Crapnell, A. G.-M. Ferrari and C. E. Banks, *Mater. Adv.*, 2022, **3**, 7632–7639.
56 J. R. Camargo, R. D. Crapnell, E. Bernalte, A. J. Cunliffe, J. Redfern, B. C. Janegitz and C. E. Banks, *Appl. Mater. Today*, 2024, **39**, 102285.
57 A. C. Oliveira, E. Bernalte, R. D. Crapnell, M. J. Whittingham, R. A. Munoz and C. E. Banks, *Appl. Mater. Today*, 2025, **42**, 102597.
58 R. D. Crapnell, E. Bernalte, E. Sigley and C. E. Banks, *RSC Adv.*, 2024, **14**, 8108–8115.
59 D. L. Ramos, R. D. Crapnell, R. Asra, E. Bernalte, A. C. Oliveira, R. A. Muñoz, E. M. Richter, A. M. Jones and C. E. Banks, *ACS Appl. Mater. Interfaces*, 2024, **16**, 56006–56018.
60 B. Ferreira, R. D. Crapnell, E. Bernalte, T. R. Paixão and C. E. Banks, *Electrochim. Acta*, 2025, **515**, 145680.
61 W. R. de Araujo, T. M. Cardoso, R. G. da Rocha, M. H. Santana, R. A. Munoz, E. M. Richter, T. R. Paixao and W. K. Coltro, *Anal. Chim. Acta*, 2018, **1034**, 1–21.
62 N. Laube, B. Mohr and A. Hesse, *J. Cryst. Growth*, 2001, **233**, 367–374.
63 C. Qian, X. Wu, F. Zhang and W. Yu, *J. Prosthet. Dent.*, 2016, **116**, 112–118.
64 S. S. Thakur, S. K. Shenoy, J. S. Suk, J. S. Hanes and I. D. Rupenthal, *Eur. J. Pharm. Biopharm.*, 2020, **148**, 118–125.
65 G. Greczynski and L. Hultman, *Sci. Rep.*, 2021, **11**, 11195.
66 E. M. Richter, D. P. Rocha, R. M. Cardoso, E. M. Keefe, C. W. Foster, R. A. Munoz and C. E. Banks, *Anal. Chem.*, 2019, **91**, 12844–12851.
67 J. Zhou, P. Yang, P. A. Kots, M. Cohen, Y. Chen, C. M. Quinn, M. D. de Mello, J. Anibal Boscoboinik, W. J. Shaw and S. Caratzoulas, *Nat. Commun.*, 2023, **14**, 2293.
68 J. Li, L. Ma, X. Li, C. Lu and H. Liu, *Ind. Eng. Chem. Res.*, 2005, **44**, 5478–5482.
69 M. Carmo, M. Linardi and J. G. R. Poco, *Appl. Catal., A*, 2009, **355**, 132–138.
70 M. H. Omar, K. A. Razak, M. N. Ab Wahab and H. H. Hamzah, *RSC Adv.*, 2021, **11**, 16557–16571.
71 J. M. Chalmers, R. W. Hannah and D. W. Mayo, *Handb. Vib. Spectrosc.*, 2002, **4**, 1893–1918.
72 Y. Wang, D. C. Alsmeyer and R. L. McCreery, *Chem. Mater.*, 1990, **2**, 557–563.
73 K. I. Hadjiivanov, D. A. Panayotov, M. Y. Mihaylov, E. Z. Ivanova, K. K. Chakarova, S. M. Andonova and N. L. Drenchev, *Chem. Rev.*, 2020, **121**, 1286–1424.
74 A. J. Bard, L. R. Faulkner and H. S. White, *Electrochemical methods: fundamentals and applications*, John Wiley & Sons, 2022.
75 P. Mehta, C. Bothiraja, K. Mahadik, S. Kadam and A. Pawar, *Biomed. Pharmacother.*, 2018, **108**, 828–837.
76 F. Ricard, E. Abe, C. Duverneuil-Mayer, P. Charlier, G. de la Grandmaison and J. C. Alvarez, *Forensic Sci. Int.*, 2012, **223**, 256–260.
77 J. Carlier, E. Escard, M. Péoc'h, B. Boyer, L. Romeuf, T. Faict, J. Guitton and Y. Gaillard, *J. Forensic Sci.*, 2014, **59**, 859–864.
78 A. Scott, *Encycl. Toxicol.*, 2014, **3**, 339–341.
79 A. C. Alves, A. D. Meinhart, J. Teixeira Filho and H. T. Godoy, *Food Sci. Technol.*, 2019, **39**, 673–682.
80 K. Hebbache, N. Ait Ahmed, N. Aliouane, C. Chassigneux and M. Eyraud, *Microchem. J.*, 2025, **213**, 113867.
81 J. V. Piovesan, C. A. de Lima, E. R. Santana and A. Spinelli, *Sens. Actuators, B*, 2017, **240**, 838–847.
82 I. Kouhi, G. Parvizi Fard, E. Alipour and A. Saadatirad, *J. Food Process. Preserv.*, 2022, **46**, e16289.